ChemComm

Accepted Manuscript

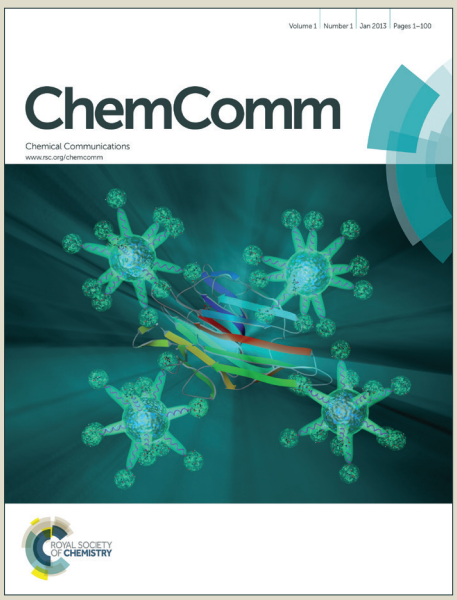

ROYAL SOCIETY OF CHEMISTRY

www.rsc.org/chemcomm

Cite this: DOI: 10.1039/c0xx00000x

www.rsc.org/xxxxxx

ARTICLE TYPE

Dual Role of Borohydride Depending on Reaction Temperature: Synthesis of Iridium and Iridium Oxide

Kalapu Chakrapani and S. Sampath*

Received (in XXX, XXX) Xth XXXXXXXXX 20XX, Accepted Xth XXXXXXXXX 20XX

DOI: 10.1039/b000000x

Temperature dependent reaction products are observed when borohydride is present in aqueous solutions containing Ir^{3+}. At temperatures of 40°C and above, metallic iridium is formed while under ambient conditions of 25°C, borohydride results in an alkaline environment that helps in hydrolyzing the precursor to form IrO_2. The Ir foams and IrO_2 are subsequently used to study their catalytic properties.

Research on small-sized metal and metal oxide nanostructures has received sufficient interest due to the unique electronic, spectroscopic, and chemical properties of the nanostructures.[1] Different morphologies have been realized by various experimental protocols.[2] Iridium metal and iridium oxide have attracted attention due to their conducting nature and hence are potential electrocatalysts.[3-5] They are also useful in other applications, for example, in hydrogen storage.[6] Ir is a promising catalyst and has been used in a variety of organic transformations such as hydrogenation and activation of C-H bonds (for hydrocarbons).[7]

Recently, porous materials particularly metals with sponge-like nanostructures have found immense applications in (electro)catalysis, hydrogen storage etc. due to their high surface area and low density.[8] Significant efforts have been directed towards the synthesis of highly porous nanostructures. Various methods proposed to realize porous nanostructures include dealloying, sol-gel processing and template techniques.[8] Noble metal nanofoams of Au, Ag, Pt and Pd have been synthesized from their corresponding chlorides using borohydride as reducing agent in aqueous media.[9] To the best of our knowledge, there is no report on highly porous Ir nanostructures. Iridium oxide has been shown to be an excellent catalyst for oxygen evolution reaction.[10,11] It has also been investigated as top-gate electrode in devices such as capacitors, ferroelectric memories and also as switching-layer in electrochromic devices.[12,13] Various synthetic procedures to prepare IrO_2 have been reported that involve hydrolysis of precursors at high temperatures,[14,15] sputtering,[16] and electrodeposition.[17] The method of preparation of nanomaterials affects the morphology and also their catalytic properties including activity and stability. Differences observed in the activity of various IrO_2 nanostructures have been reported to be due to availability of active sites on the surface, volume fraction of hydrated layers vs. compact oxides and of course the crystallinity of the materials.[18] A recent report that highlights the synthesis of both Ir and IrO_2 thin films, uses atomic layer deposition technique.[19] However, this method requires ozone and hydrogen gas, the deposition rate is generally low and the cost of the experimental set-up is high.

The present study reports the tuning of the synthesis of iridium and iridium oxide depending on the reaction conditions used. The synthesis involves the reduction or hydrolysis of the iridium precursor depending on the temperature. The reductant takes a dual role (i.e.) acts as reducing agent for the formation of iridium nanoparticles when used at temperatures of 40°C and above while hydrolysis of the precursor helps in increasing the pH of the medium, forming iridium oxide, when used at 25°C. The Ir nanostructures have been investigated as catalysts for the reduction of nitroaromatics in the presence of borohydride and the iridium oxide particles are tested as catalyst for oxygen evolution reaction. The details of preparation conditions are given in the supporting information.

Morphological investigations of the samples (figure 1) show Ir foam-like structures for the material prepared at 80°C. Low magnification FESEM image shows similar morphology of Ir nanofoams. The nanofoams are composed of porous, interlaced and interconnected networks of particles as shown in figure 1B. The size of individual nanoparticles is in the range of 20-50 nm and is not very uniform. The TEM images (figure 1C) show that the network is assembled to form granular nanocrystals. The cross linking of the networks leads to the formation of foam-like structures. The HRTEM image gives information on micro-structure of nanofoams and the lattice constant observed is 0.23 nm corresponding to {111} plane of fcc Ir (figure 1D).

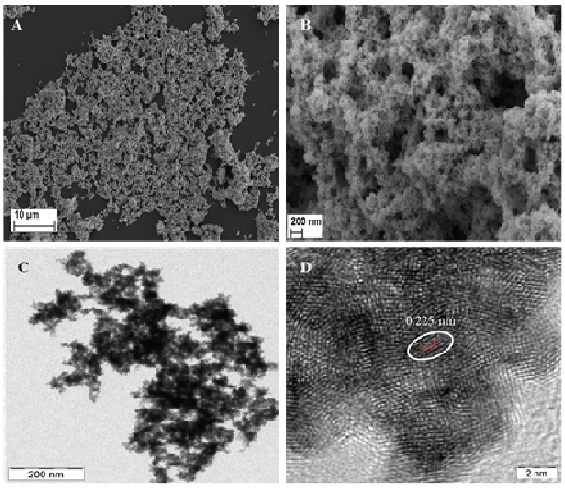

Figure 1. (A,B) Scanning electron microscopy, (C) Transmission electron microscopy (TEM) images and (D) high resolution TEM of Ir nanofoams. Ir foams are prepared by reducing Ir^{3+} using borohydride at 80°C for 5 minutes.

Selected area electron diffraction (SAED) patterns shows highly crystalline Ir reflections (figure S1). The energy dispersive analysis confirms the presence of only Ir (figure S2). Figure 2A shows the XRD pattern of Ir nanofoams. It is observed that the sample is highly crystalline, showing dominant diffractions observed at 2θ values of 40.9, 47.2, 69.1 and 83.6 degrees and the diffraction peaks are assigned to {111} {200} {220} {311} facets of Ir fcc structure.[19] There is no oxide formation observed in the XRD pattern.

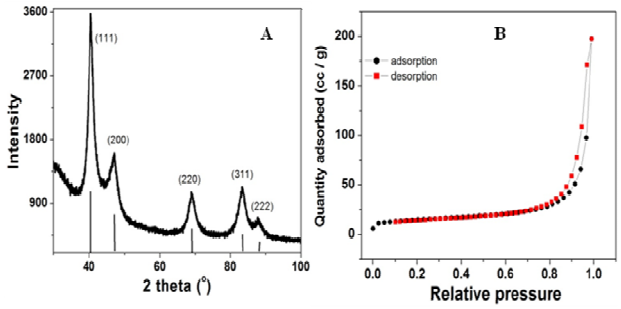

Figure 2. (A) X-ray diffraction pattern and (B) N_2 adsorption-desorption isotherm (77K) of Ir nanofoams using BET method.

Surface area analysis is carried out by BET method using N_2 adsorption-desorption isotherm at 77 K (figure 2B) and the surface area of Ir nanofoams is found to be 24.3 m^2/g. The observed surface area for Ir foams is reported for the first time and almost similar to other noble metal foams.[9] To our knowledge, Ir foams have not been reported in the literature. XPS analysis has been carried out in order to ascertain the chemical state of as-obtained Ir foams. Figure S3 shows the core level X-ray photoelectron spectrum of Ir 4f region. The spectrum is composed of two pairs of doublets. The predominance of zerovalent Ir peaks observed at 61.1 and 64.1 eV correspond to Ir $4f_{7/2}$ and Ir $4f_{5/2}$ levels with small fraction of surface oxides observed at 62.3 and 65.4 eV.[6]

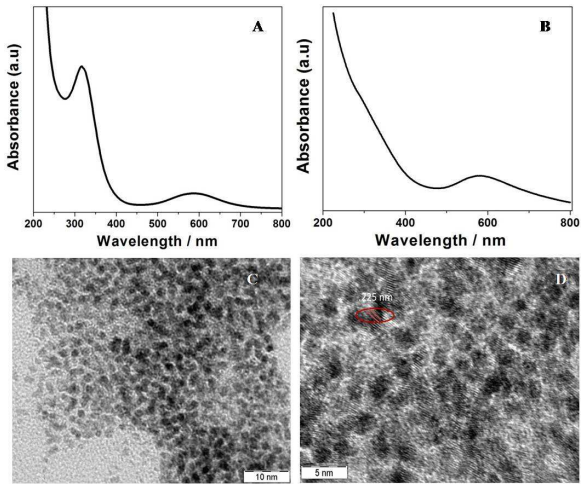

Figure 3. UV-Vis absorption spectrum of IrO_2 (A) shows the as-prepared particles and (B) after annealing at 100°C for 2 hours. (C) Transmission electron microscopy (TEM) images and (D) high resolution TEM of IrO_2.

The same reaction carried out at different reaction temperatures of 40°C and above shows dominant XRD peaks that correspond to fcc Ir structure (figure S4). The same reaction carried out at 25°C does not result in the formation of Ir (i.e) reduction of Ir precursor in presence of sodium borohydride does not proceed. Similar observations have been reported earlier where Ir (0) nanoparticles are not formed under ambient conditions with addition of even 10 fold excess of borohydride and also under H_2 atmosphere.[20] When Ir^{3+} precursor is treated with $NaBH_4$ at 25°C, the colour of the solution changes to blue after quite some time, ~ 40 hours. The observed change in colour is found to be due to the formation of IrO_2, which possesses a characteristic deep blue colour. UV-Vis spectroscopic studies are carried out to follow the course of formation of IrO_2 after the addition of borohydride. Figure 3A shows an absorbance at 574 nm, characteristic of IrO_2 while a strong band observed at 315 nm corresponds to monomeric $\{Ir(OH)_6\}^{2-}$.[21] Formation of this complex is due to the hydrolysis of Ir-Cl bond. When the centrifuged sample is annealed at 100°C, the peak at 315 nm disappears due to the conversion of hydrated iridium oxide to crystalline IrO_2. UV-Vis spectrum of the annealed sample in aqueous medium shows an absorption band at 575 nm (figure 3B) corresponding to the electronic transition between t_{2g} and e_g orbitals of Ir present in (IV) state in a distorted octahedral coordination environment, whereas a sharp increase in absorbance below 400 nm is associated with the ligand to metal transition (i.e) O 2p to Ir 5d levels. It is reported that the iridium precursor gets hydrolyzed at basic pH (~ 13) and at 80°C forming IrO_2[22] while at pH ~ 10 solutions, the formation of IrO_2 takes 4 days at 37°C.[23]

During the course of the reaction, the pH of the solution is monitored and it is observed that before the addition of borohydride, the pH of the solution is ~ 4.1 and once borohydride is added, the pH increases to ~ 10.5 and remains constant for a long time. It is likely that sodium borohydride hydrolyzes in water to form (BO_2^{-1}) metaborate ion. This increases the pH of the solution where iridium trichloride hydrolyzes to form hydrated iridium oxide and subsequently iridium oxide.

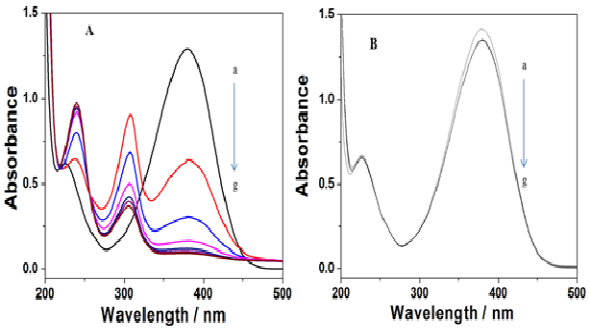

Figure 4. UV-Vis spectra for p-NA reduction at different time intervals. (A) $NaBH_4$ + Ir foams and (B) $NaBH_4$ + IrO_2. Experimental conditions: concentration of p-NA and NaBH4 are 0.3 mM and 10 mM; concentration of Ir foams and IrO_2 are 1 µM and 500 µM. The time intervals are (a) immediately after the reaction mixture is prepared (b) 3; (c) 6; (d) 9; (e) 12; (f) 15 and (g) 20 minutes of reaction.

The hydrolysis in the presence of borohydride may be due to a change in alkalinity of the solution. Figure S5 shows the XRD patterns of IrO_2 before and after annealing the samples at 400°C for 3 hours in air. The amorphous material after annealing at 400°C, shows diffraction peaks at 28°, 34°, 40° and 54° corresponding to (110), (101), (200), and (211) planes of rutile IrO_2 in the tetragonal phase (JCPDS 88-0288). It has been reported that IrO_2 synthesized using chemical hydrolysis route are amorphous in nature and crystallinity is observed after annealing at high temperatures.[24]

XPS technique is used to understand the surface composition and chemical state of the sample. Figure S6 shows the XPS spectrum of IrO_2 in Ir 4f region. The peaks located at binding energy values of 62.1 eV and 64.9 eV correspond to Ir $4f_{7/2}$ and Ir $4f_{5/2}$ levels of Ir^{4+}. The Raman spectrum (figure S6) reveals characteristic peaks at 557, 729 cm^{-1} attributed to the first order E_g, B_{2g} phonon Raman bands of rutile IrO_2 structure. The observed band frequencies correspond to the measured values on bulk samples and the recently reported IrO_2 nanowires.[25] Transmission electron microscopy (TEM) images show the nanoparticles are of very small size (figure 3C). High resolution TEM (HRTEM) images show lattice constant of 0.225 nm corresponding to (101) plane of rutile IrO_2.

Though the redox potential values suggest that the reduction of Ir (III) to Ir (0) should be feasible in presence of borohydride (supporting information), the experimental observations are different. It is quite well documented that borohydride undergoes hydrolysis to form various complex species and use of strong reducing agents such as Cu, Mg, Zn and also borohydride does not help in reducing Ir ions under ambient conditions.[26-32] Some of the ionic equilibria that exist during borohydride hydrolysis involve, BH_4^- / $BH_3(OH)^-$; $BH_3(OH)^-$ /$BH_2(OH)_2^-$; $BH_2(OH)_2^-$/ $BH(OH)_3^-$ and $BH(OH)_3^-$/$B(OH)_4^-$ simultaneously.[31] The reduction of metal ions using borohydride should take in to account the redox potentials of all the species formed during the hydrolysis of BH_4^-. In addition, the hydrolysis of Ir (III) species results in several complexes as given below.[29]

$$[Ir(OH_2)_6]^{3+} \text{ ===== } [Ir(OH_2)_5(OH)]^{2+} + H^+$$

$$[Ir(OH_2)_5\,(OH)]^{2+} \text{ ==== } [Ir(OH_2)_4(OH)_2]^{+} + H^+$$

$$[Ir(OH_2)_3(OH)_3](s) + 3H^+ \text{ ==== } [Ir(OH_2)_6^{3+}$$

The third aspect is related to the release of hydrogen during borohydride hydrolysis. All the three points mentioned above, (i.e) hydrolysis of borohydride, hydrolysis of Ir(III) and release of hydrogen would dictate the product formed at different temperatures. The amount of hydrogen released during hydrolysis of borohydride increases drastically as a function of temperature.[31] Hence, it is likely that the rate of release of hydrogen being low under ambient conditions probably results in the hydrolysis of Ir(III) leading to IrO_2 while at higher temperatures, the relative rates of all the reactions given above become a deciding factor. It is also observed that the products do not coexist after the completion of the reaction at different temperatures. It should also be emphasized that the product is IrO_2 when Ir(III) is reacted at 25°C in an alkaline solution of NaOH without borohydride. This confirms that it is just the alkalinity that is responsible for the formation of IrO_2 at 25°C while it is the presence of borohydride that is required to form Ir (0) at higher temperatures. Another point that requires clarification is the formation of Ir(IV) species from Ir (III) when IrO_2 is formed at 25 C. It has been suggested [33,34] that both base and oxygen are responsible for the formation of Ir (IV) species through Ir_2O_3 when Ir (III) is hydrolysed (supporting information).

Hence, borohydride plays a dual role during the synthesis of Ir nanostructures where IrO_2 and Ir are formed, one where borohydride acts as a reducing agent (formation of Ir) while the other role is where borohydride hydrolyzes in water increasing the pH of the medium that in turn helps hydrolyze $IrCl_3$ form IrO_2.

The catalytic activity of Ir and IrO_2 nanostructures are compared using the reduction of p-nitroaniline in the presence of borohydride. This reaction is one of the model reactions for evaluating the catalytic activity of various noble metals such as Au, Ag, Pt, and Rh.[35-39] However, catalytic activity of iridium nanostructures for this conversion is not reported. The reduction of p-NA in the presence of borohydride is thermodynamically favoured but it is kinetically restricted without a catalyst. In the absence of any reagent except borohydride, the reduction is very slow as shown in figure S7 which reveals only 2-3% of conversion even after 48 hours. Similarly, it is found that the reduction of p-NA in the presence of Ir without $NaBH_4$ does not proceed. It is important that a proper combination of catalyst and borohydride is necessary for the reaction to occur at reasonable kinetics. After the addition of Ir foams, the reduction of p-NA is fast and the conversion is complete within 15 minutes. Figure 4A shows that the absorption peak corresponding to p-NA at 380 nm decreases and disappears after 12 minutes and a new peak is observed at 307 nm that is due to the reduced product. Of the metallic catalysts that have been reported for this reaction, Au and Ag show rate constants one order less than that of Ir nanostructures which is close to that of Pd and Pt catalysts. Similar experiments carried out using IrO_2 shows that it is

inefficient for the reduction of p-NA (figure 4B).

In conclusion, nanostructures of Ir and IrO_2 have been synthesized using a simple protocol. The present study has explored the use of borohydride as a reducing agent at high temperatures to form high surface area Ir foams and as a reagent to change the pH of the solution at 25°C to forms IrO_2. The porous Ir foams show efficient catalytic activity for the reduction of p-NA in the presence of excess borohydride.

Notes and references

Department of Inorganic and Physical Chemistry, Indian Institute of Science. Bangalore 560012, India. Fax: +91-80-2360-0085: Tel:+91-80-2293-3315; E-mail: sampath@ipc.iisc.ernet.in

†Electronic Supplementary Information (ESI) available: Detailed experimental procedures for the preparation of Ir nanostructures. SAED pattern, TEM, XRD, XPS, Raman and surface area (BET) data of Ir and IrO_2 nanostructures

1. R. S. Devan, R. A. Patil, J. H. Lin and Y. R. Ma, *Adv. Funct. Mater.,* 2012, **22,** 3326.
2. J. P. Breen, R. Burch, J. Gomez-Lopez, K. Griffin and M. Hayes, *Appl. Catal. A,* 2004, **268,** 267.
3. K. Chakrapani and S. Sampath, *Phys. Chem. Chem. Phys.,* 2014, **16,** 16815.
4. K. Chakrapani and S. Sampath, *Chem. Commun.,* 2014, **50,** 3061
5. V. Kiran, T. Ravi Kumar, N. T. Kalyanasundaram, S. Krishnamurthy, A. K. Shukla and S. Sampath, *J. Electrochem. Soc.,* 2010, **157,** B1201.
6. H. Kobayashi, M. Yamauchi and H. Kitagawa, *J. Am. Chem. Soc.,* 2012, **134,** 6893.
7. E. Bayaram, M. Zahmakiran, S. Ozkar and R. G. Finke, *Langmuir,* 2010, **26** 12455.
8. B. C. Tappan, S. A. Steiner III and E. P. Luther, *Angew. Chem. Int. Ed.,* 2010, **49,** 4544.
9. K. S. Krishna, C. S. Sandeep, R. Philip and M. Eswaramoorthy, *ACS Nano,* 2010, **4,** 2681.
10. Y. Lee, J. Suntivich, K. J. May, E. E. Perry and Y. Shao-Horn, *J. Phys. Chem. Lett.,* 2012, **3,** 399.
11. S. J. Kwon, F. R. F. Fan and A. J. Bard, *J. Am. Chem. Soc.,* 2010, **132,** 13165.
12. K. K. Abdelghafar, M. Hiratani and Y. Fujisaki, *J. Appl. Phys.,* 1999, **85,** 1069.
13. T. Nakamura, Y. Nakao, A. Kamisawa and H. Takasu, *Appl. Phys. Lett.,* 1994, **65,** 1522.
14. A. A. Gamberdella, S. W. Feldberg and R. W. Murray, *J. Am. Chem. Soc.,* 2012, **134,** 5774.
15. P. G. Hoertz, Y. Kim, W. J. Youbgblood and T. E. Mallouk, *J. Phys. Chem. B,* 2007, **111,** 6845**.**
16. J. D. Weiland and D. J. Anderson, *IEEE. Trans. Biomed. Eng.,* 2000, **47,** 911.
17. P. Steegastra and E. Ahlberg, *Electrochim. Acta,* 2012, **76,** 26.
18. M. N. Kushner-Lenhoff, J. D. Blakemore, N. D. Schley, R. H. Crabtree and G. W. Brudvig, *Dalton.Trans.,* 2013, **42,** 3617.
19. J. Hamalainen, V. Hatanpaa, E. Puukilainen, T. Sajavaara, M. Ritalaa and M. Leskelaa, *J. Mater. Chem.,* 2011, **21,** 16488.
20. Y. M. Lopez-De Jesus, A. Vincente, G. Lafaye, P. Marecot and C. T. Williams, *J. Phys. Chem. C,* 2008, **112,** 13837.
21. Y. Zhao, E. A. Hernandez-pagan, N. M. Vargas-Barbosa, J. L. Dysart and T. E. Mallouk, *J. Phys. Chem. Lett.,* 2011, **2,** 402.
22. M. Yagi, E. Tomita, S. Sakita, V. Kuwabara and K. Nagai, *J. Phys. Chem. B,* 2005, **109,** 21489.
23. A. M. Cruz, L. Abad, N. M. Carretero, J. Moral-Vico, J. Fraxedas, P. Lozano, G. Subias, V. Padial, M. Carballo, J. Collazos-Castro and N. Casan-Pastor, *J. Phys. Chem. C,* 2012, **116,** 5155.
24. C. C. Chang, T. C. Wen, C. H. Yang and J. D. Juang, *Mater. Chem. Phys.,* 2009, **115,** 93.
25. J. H. Shim, Y. Lee, M. Kang, J. Lee, J. M. Baik, Y. Lee, C. Lee and M. H. Kim, *Anal. Chem.,* 2012, **84,** 3827.
26. G. G. Tertipis and F. E. Beamish, *Anal. Chem.,* 1960, **32**, 486.
27. E. S. Mckay and R. W. Cordrell, *Talanta*, 1971, **18**, 841.
28. D. F. C. Morris and T. J. Ritter, *Hydrometallurgy*, 1978, **3**, 297.
29. H. Gamsjäger and P. Beutler, *J. Chem. Soc. Dalton Trans.*, 1979, 1415.
30. J. Andrieux, U. B. Demirci, J. Hannauer, C. Gervais, C. Goutaudier and P. Miele, *Int J. Hydrogen Energy*, 2011**, 36**, 224.
31. R. Retnamma, A. Q. Novais and C. M. Rangel, *Int J. Hydrogen Energy*, 2011, **36**, 9772.
32. H. I. Schlesinger, H. C. Brown, A. E. Finholt, J. R. Gilbreath, H. R. Hoekstra and E. K. Hyde, *J. Am. Chem. Soc.*, 1953, **75**, 215.
33. L. Wöhler and W. Witzmann, *Zeitschrift für Anorganische Chemie*, 1908, **57**, 323.
34. A. Harriman, J. M. Thomas and G. R. Millward, *New J. Chem.* 1987, **11**, 757.
35. S. Wunder, F. Polzer, Y. Lu, Y. Y. Mei and M. Ballauff, *J. Phys. Chem. C,* 2010, **114,** 8814.
36. Y. Gao, X. Ding, Z. Zheng, C. Cheng and Y. Peng, *Chem. Commun.,* 2007, 3720.
37. S. Praharaj, S. Nath, S. K. Ghosh, S. Kundu and T. Pal, Langmuir*,* 2004, **20,** 9889.
38. S. Kundu, K. Wang and H. Liang, *J. Phys. Chem. C,* 2009, **113,** 18570.
39. J. Zeng, Q. Zhang, J. Chen and Y. Xia, *Nano Lett.,* 2010, **10,** 30.